Technical note: Towards a stronger observational support for haze pollution control by interpreting carbonaceous aerosol results derived from different measurement approaches

Yuan Cheng, Ying-jie Zhong, Zhi-qing Zhang, Xu-bing Cao, Jiu-meng Liu*

State Key Laboratory of Urban Water Resource and Environment, School of Environment, Harbin Institute of Technology, Harbin, 150090, China

* Corresponding author. Jiu-meng Liu (jiumengliu@hit.edu.cn).

Abstract

As China's fine particulate matter ($PM_{2.5}$) has decreased nationwide during the last decade, further improvement of air quality became more challenging, imposing higher requirements on the observational support for the understanding of aerosol sources. This was particularly the case for the severe cold climate region in Northeast China, which suffered from relatively slow decreasing rate and high exposure risk of $PM_{2.5}$. Here we evaluated carbonaceous aerosol data measured by different sampling and analytical approaches, based on field campaigns conducted during a frigid winter and an agricultural-fire impacted spring in Harbin. For both the high- and low-volume sampling, a total of four sets of organic and elemental carbon results were derived by applying two commonly-used temperature protocols (IMPROVE-A, i.e., IMPV, and NIOSH) to both untreated filters and those extracted by methanol. Only the IMPV-based results measured before the extraction were found to be indicative of aerosol sources, e.g., in reasonable accordance with secondary aerosol formation in winter and open burning impacts in spring. Thus the analytical method of IMPROVE-A on untreated samples was recommended for future field observations and source apportionments of $PM_{2.5}$ in the studied region. In addition, although the low- and high-volume samplers typically led to comparable measurement results for various species, exceptions were identified for water-soluble potassium (K^+) and some fire-emitted chromophores. We suggested that K+ and light

absorption coefficients of brown carbon should be compared or integrated with caution across studies using different $PM_{2.5}$ samplers. ~~K^+ detected by different $PM_{2.5}$ samplers may not be directly comparable, and K^+ should be used with caution as a biomass burning tracer for studies relying on high-volume measurements~~.

1. Introduction

Carbonaceous aerosols are a complex mixture of compounds exhibiting a gradual change in chemical and physical properties (Pöschl, 2005; Andreae and Gelencsér, 2006), e.g., from colorless organics with low molecular weights, to "dark" brown carbon with relatively high thermal stabilities (Chakrabarty et al., 2023), and finally to refractory black carbon which is strongly light-absorbing. As important contributors to both fine particulate matter ($PM_{2.5}$) pollution and radiative forcing, they have long been targeted to achieve a synergistic improvement of air quality and mitigation of climate change (Fuzzi et al., 2015; von Schneidemesser et al., 2015; Liu et al., 2022). However, it remains a challenge to properly represent carbonaceous aerosols in chemical transport models, as each step along the way between the estimations of sources and tempo-spatial variations is difficult. For example, considerable uncertainties exist in the open burning emission, secondary organic aerosol (SOA) budget and black carbon lifetime (Andela et al., 2022; Chang et al., 2022; Zhong et al., 2023). This in turn introduces substantial uncertainties to the climate and health effects of carbonaceous aerosols (Li et al., 2022).

Field observational data on carbonaceous aerosols, including those derived from ground and aircraft measurements, are essential to constrain the simulation results and subsequently to improve the model performance (Philip et al., 2014; Wang et al., 2014b, 2018; Gao et al., 2022; Eckhardt et al., 2023). Relying on on-line instruments such as the Single Particle Soot Photometer (SP2), aircraft studies typically covered relatively short periods (e.g., up to about one month) but provided measurement results with high time and spatial resolutions (Samset et al., 2014). Offline and semi-continuous techniques (e.g., lab and field carbon analyzers for elemental carbon) were more commonly used in ground observations, ~~giving rise to~~ producing datasets with relatively low time

resolutions but spanning several months to decades (Dao et al., 2019; Hand et al., 2024). After accounting for the difference in time resolution, the integration of carbonaceous aerosol data across studies and regions was still not straightforward. A major obstacle was caused by the multitude of measurement principles (Petzold et al., 2013), which was intensively reflected by the considerable and, more importantly, variable discrepancies in black carbon results among different methods (Buffaloe et al., 2014; Li et al., 2019; Pileci et al., 2021; Tinorua et al., 2024). This problem was far from being properly addressed, although great efforts have been devoted to refine the respective measurement approach such as the thermal-optical (Cavalli et al., 2010), optical (Collaud Coen et al., 2010) and SP2 (Laborde et al., 2012) techniques. In addition, this problem was to some extent overlooked in China, which might be partially responsible for the inconsistent source apportionment results obtained by different studies. For example, both Zheng et al. (2015) and Liu et al. (2020) applied the ~~EC~~ elemental carbon (EC) tracer method to estimate secondary OC (SOC) during winter in Beijing, but the two studies derived conflicted conclusions on the contribution of heterogeneous chemistry to SOC formation (i.e., minimal vs. significant) since different analytical methods (i.e., NIOSH vs. IMPROVE-A temperature protocols) for EC were deployed. Such inconsistencies substantially weakened the observational support for the understanding of aerosol sources and thus the control of haze pollution.

With a considerable decrease in the national $PM_{2.5}$ since 2013, it became more challenging to further improve the air quality in China (Cheng et al., 2021). This imposed higher requirements on the observational insights into aerosol sources, including the evaluation of carbonaceous aerosol results among various measurement approaches. Here we focused on the widely-used thermal-optical method, which separates carbonaceous components into two fractions with different thermal

stabilities and light absorption capacities, i.e., organic carbon (OC) and ~~elemental carbon (~~EC~~)~~. The basis of the separation includes two points: EC ~~survives to~~ evolves form the filter at higher temperatures than OC, and the removal of EC leads to a rapid increase in the filter transmittance and reflectance signals. A major problem in this method is that a considerable fraction of OC could be transformed into char-OC, which is difficult to be robustly distinguished from EC with respect to either thermal or optical behavior. In addition, the amount and optical properties of char-OC were found to depend on the temperature protocol deployed (Yu et al., 2002; Yang and Yu, 2002; Subramanian et al., 2006). This to a large extent explained the EC discrepancies among various protocols. However, it remained unclear how the charring process and thus the EC measurement were influenced by OC sources and composition (Chiappini et al., 2014). In addition, to reduce or minimize the interference from char-OC, several investigators have tried to remove a fraction of OC from the samples before thermal-optical analysis, by extracting the filters using water, methanol or other solvents (Piazzalunga et al., 2011; Giannoni et al., 2016; Lappi and Ristimäki, 2017; Aakko-Saksa et al., 2018; Hu et al., 2023). However, inconsistent patterns were identified for the effects of OC removal on EC determination, with evidences available for both an increase (e.g., Piazzalunga et al., 2011) and a decrease in EC (e.g., Hu et al., 2023) after the extraction. The discussions above indicated that the thermal-optical methods, including the practicability of sample pretreatment by extraction, merit further investigations.

In this study, we compared carbonaceous aerosol results determined by different analytical as well as sampling approaches, based on filter samples collected in Harbin, the northernmost megacity in China. Compared to other megacities such as Beijing, Harbin is characterized by the frigid winter (with an average temperature of about –20 °C in January) and the massive agricultural sector in

surrounding areas (i.e., the Songnen Plain in Northeast China). In addition, Harbin and other cities in Northeast China have largely been overlooked in clean air actions and thus studies on haze, as indicated by the limited observational data available (Liu et al., 2022). This lack of investigation was partially responsible for the relatively slow decreasing rate (Xiao et al., 2022) and high exposure risk (Wei et al., 2023) of $PM_{2.5}$ in this distinct region. Thus our study on measurement methods of carbonaceous aerosols is expected to be a support for future efforts on the exploration of ~~the~~ $PM_{2.5}$ sources in Northeast China, which are essential for further improving the regional air quality.

2. Methods

2.1 Field sampling

$PM_{2.5}$ samples were collected at an urban site in Harbin, i.e., on the campus of Harbin Institute of Technology ~~(HIT)~~, during the winter and spring of 2021. The sampling was done by a mass flow controlled high-volume sampler (TE-6070BLX-2.5-HVS; Tisch Environmental, Inc., OH, USA) and a low-volume sampler (MiniVol; Airmetrics, OR, USA), operated using quartz-fiber filters (Pall Corporation, NY, USA) at flow rates of 1.13 m^3/min and 5 L/min, respectively. The flow rates, together with the particle-laden filter areas, could be translated into the face velocities of 46.34 and 7.35 cm/s for the high- and low-volume (HV and LV) samplers, respectively. This indicated that when the two samplers were run in parallel, the HV-to-LV ratio of particle loading would be 6.3.

The 2021 winter campaign covered the entirety of January, the coldest month during that year with an average temperature of –19 °C.~~, whereas the~~ In addition, the spring campaign was conducted during 10–30 April of 2021, a period with frequent occurrences of agricultural fires (as indicated by the satellite-based active fire detection results; Figure S1). For both seasons, the HV sampler was used to collect daytime (09:00–16:00) and nighttime (21:00–05:00 of the next day) samples, while

the LV one was operated on a daily basis (~09:00–09:00 of the next day), leading to 24-h integrated samples. Each LV sample generally corresponded to two HV samples, although the two samplers were not exactly parallel. One reason for the relatively short sampling durations of HV was to avoid ~~extremely~~ high particle loadings that could prohibit proper filter transmittance measurement ~~which could make the filters unsuitable for thermal-optical analysis~~ (Lappi and Ristimäki, 2017).

2.2 Laboratory analysis

For both the HV and LV samples, two punches were prepared to determine OC and EC using a thermal-optical carbon analyzer (DRI-2001; Atmoslytic Inc., CA, USA). One punch was directly measured, while the other one was immersed in methanol (HPLC grade; Fisher Scientific Company L.L.C., NJ, USA) for an hour without stirring or sonication, dried in air for another hour, and then analyzed. All the pairs of untreated and extracted punches were measured using the IMPROVE-A and NIOSH temperature protocols, both of which were operated with transmittance charring correction (Figure 1). This correction approach was applied since the intensity of the filter transmittance signal (I) has a clear association with EC, e.g., as assumed by the Aethalometer, another widely used instrument for measuring black carbon. Inter-protocol comparisons showed good repeatability for both the total carbon (TC) and optical attenuation (ATN) results (Figure 2), demonstrating the robustness of the analyzer for detecting carbon and filter transmittance signals ~~(I)~~. Here ATN was calculated as $\ln(I_{final}/I_{initial})$, where $I_{initial}$ and I_{final} indicate I measured at beginning (i.e., when the particle-laden filter has not been heated) and end (i.e., when all the deposited carbon has been combusted off the filter) of thermal-optical analysis, respectively. ATN was of interest because it was closely related to EC loading (EC_s, in μg/cm^2), e.g., typically with a linear dependence for relatively low EC_s levels (Chen et al., 2020; Liu et al., 2020). It should be noted that

for the parallel TC and ATN measurements by different protocols, the relative standard deviation (RSD) levels indeed increased after the extraction, e.g., from ~2 to 5% and from ~2 to 4% for the HV samples, respectively. However, the RSD levels, i.e., the uncertainties, were considered low enough for both the untreated and extracted filters.

In addition, following the method developed by Hecobian et al. (2010), wavelength-resolved light absorption coefficients (b_{abs}) of the methanol extracts, i.e., the dissolved brown carbon (BrC), were measured using a spectrophotometer (Ocean Optics Inc., FL, USA) coupled with a 2.5-m long liquid waveguide capillary cell (LWCC; World Precision Instruments, FL, USA). Inorganic ions and levoglucosan were also determined for the HV and HV samples, by analyzing their water extracts using a Dionex ion chromatography system (ICS-5000$^+$; Thermo Fisher Scientific Inc., MA, USA).

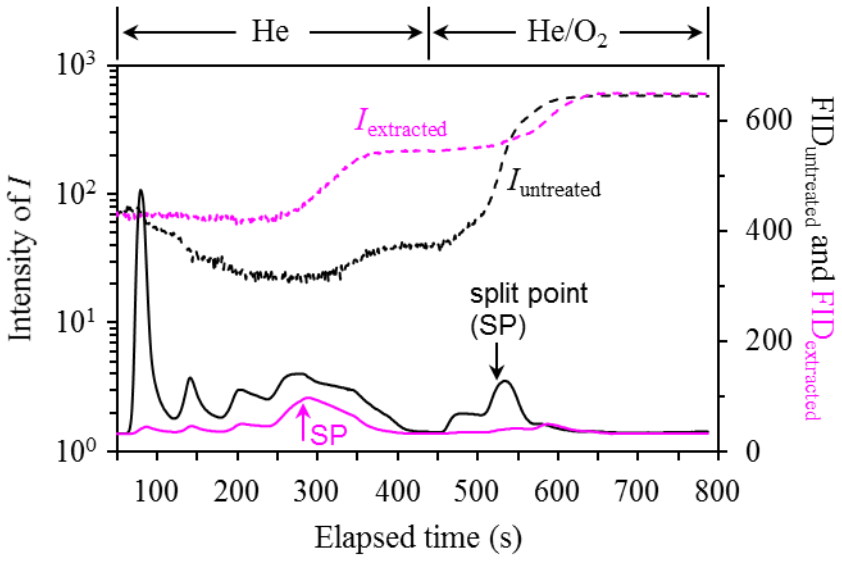

Figure 1. Thermograms measured using a pair of untreated and extracted HV filters. The sample was collected during the daytime of 25 January, 2021. Temperature protocol used was NIOSH, in which the filter was heated in a He (first to 870 ℃ stepwise and then cooled down to 550 ℃) and a He/O_2 (from 550 to 890 ℃ stepwise) atmosphere sequentially. NIOSH had fixed durations for the various heating stages and thus was preferred for the comparison of thermograms. *I* indicates the filter transmittance signal; FID indicates the carbon signal, which was measured by a flame ionization detector. The subscripts "untreated" and "extracted" distinguished the thermograms measured before and after the extraction, while the split points of OC and EC were marked by the arrows.

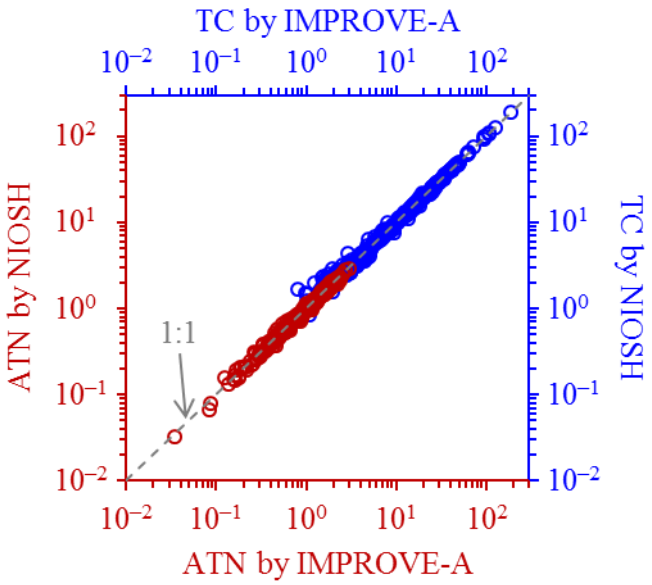

158

159 **Figure 2.** Comparisons of TC (in μgC/cm^2) and ATN (dimensionless) measured using different
160 temperature protocols. Results from the HV and LV samples, both untreated and extracted, were
161 combined for the comparisons. Linear regression of the NIOSH-based TC on that determined by
162 IMPROVE-A led to a slope of 0.99 ± 0.00 (r = 1.00; intercept was set as zero). Similar regression
163 results (i.e., slope = 0.99 ± 0.00; r = 1.00) were obtained for ATN. The good repeatabilities on one
164 hand demonstrated the performance of carbon analyzer for measuring the carbon and laser
165 transmittance signals, and on other hand indicated a homogeneous distribution of carbonaceous
166 components for not only the untreated but also the extracted filters, i.e., a negligible disturbance of
167 EC as well as other insoluble carbon by the extraction.

168 **2.3 Open-access data**

169 Meteorological data (e.g., temperature and relative humidity) and air quality data (e.g., $PM_{2.5}$,
170 PM_{10} and CO) for the measurement periods were obtained with a time resolution of 1 h from
171 Weather Underground (https://www.wunderground.com/) and the China National Environmental
172 Monitoring Center (CNEMC; https://air.cnemc.cn:18007/), respectively.

173 **3. Results and discussion**

174 **3.1 Evaluation of EC results from the winter campaign**

175 A precondition for proper separation of OC and EC is that the filter transmittance signal (I)
176 could properly reflect the formation of light-absorbing char-OC during the inert mode (which would
177 result in a decrease in I), and the combustion, i.e., removal, of char-OC and EC during the oxidation

178 mode (which would result in an increase in *I*). An empirical approach to evaluate this precondition
179 is to examine the dependence of ATN on EC_s (Subramanian et al., 2006). A linear relationship was
180 typically observed for relatively low EC_s levels and in this case, the precondition was commonly
181 believed to be valid. However, the linearity did not necessarily extend when EC_s further increased,
182 since previous studies frequently found that the measured ATN could be considerably lower than
183 expected for heavily-loaded samples (Shen et al., 2013; Costa et al., 2016; Chen et al., 2020). The
184 deviation of ATN vs. EC_s dependence from linear relationship was usually termed the loading effect,
185 and a traditional explanation was that ATN became less sensitive to the variation of EC_s as filter
186 loading increased. An extreme case was observed during winter in Beijing, that the ATN values
187 were largely unchanged for heavily-loaded filters with TC varying between 150 and 300 μgC/cm^2
188 (Liu et al., 2019). For the samples showing non-linear ATN vs. EC_s dependence, their EC results
189 should be interpreted with caution.

190 We first investigated the relationship between ATN and EC_s for the wintertime HV samples,
191 focusing on the results from IMPROVE-A. For the untreated filters, ATN correlated linearly with
192 EC_s (leading to a regression slope of 42.8 ± 1.9 m^2/gC and a close-to-zero intercept; r = 0.95) when
193 the filters were lightly to moderately loaded, i.e., when the EC_s levels were below 5 μgC/cm^2 (Figure
194 3a). The physical meaning of the slope was the mass absorption efficiency (MAE) of black carbon,
195 but with artifacts such as that caused by the multiple scattering effect (Lack et al., 2014). The overall
196 impact of various artifacts results in an overestimation of MAE, typically by factors of ~3 (Knox et
197 al., 2009; Qin et al., 2018). The linearity determined for the EC_s range of below 5 μgC/cm^2 did not
198 hold for the more heavily loaded samples (N = 3, as highlighted by the solid circles in Figure 3a),
199 showing evidence for the loading effect. For the extracted samples, a linear correlation between

ATN and EC_s was also identified for relatively low EC loadings (Figure 3b), with a similar relationship (i.e., a regression slope of 41.5 m^2/gC and a close-to-zero intercept; r = 0.95) to that derived from the untreated filters. However, it was noteworthy that EC_{max}, the upper limit of EC loading for a linear ATN vs. EC_s dependence, was only 3 $\mu gC/cm^2$ for the extracted filters, much lower than that determined for the untreated ones. Due to the shift of EC_{max}, 51% of the extracted samples showed evidence for the loading effect, whereas this fraction was only 5% before extraction.

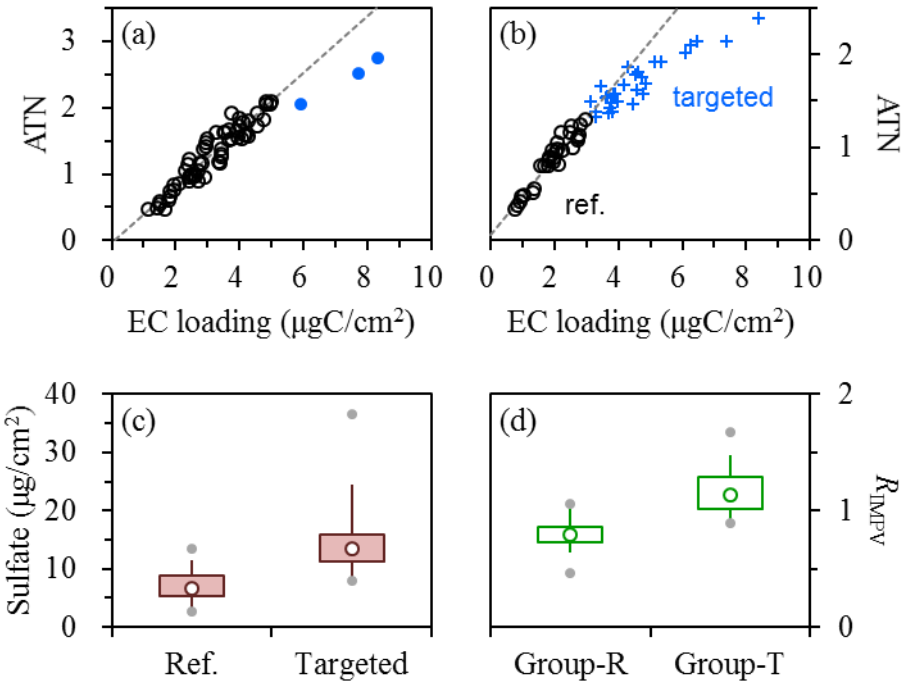

Figure 3. Relationships between ATN and EC loading, i.e., EC_s, for the **(a)** untreated and **(b)** extracted HV filters collected in winter, using the IMPROVE-A protocol. Linear dependences were observed for the untreated samples with EC_s below 5 $\mu gC/cm^2$ and for the extracted samples with EC_s below 3 gC/cm^2, as indicated by the dashed lines in (a) and (b), respectively. Three untreated samples had EC_s above 5 $\mu gC/cm^2$, as highlighted by the solid circles in (a). In (b), the extracted filters showing non-linear ATN vs. EC_s dependence were termed ~~as~~ the targeted samples; correspondingly, the others were referred to as the reference ones (labelled as ref.). **(c)** Comparison of sulfate loadings between the reference and targeted samples. **(d)** Comparison of the $EC_{extracted}$ to $EC_{untreated}$ ratios, i.e., R_{IMPV}, between the reference and targeted groups of wintertime HV samples (labelled as Group-R and Group-T, respectively). The targeted group indicated the targeted filters and the corresponding untreated ones, while the reference group indicated the remaining pairs. Lower and upper box bounds indicate the 25th and 75th percentiles, the whiskers below and above the box indicate the 5th and 95th percentiles, the solid circles below and above the box indicate the minimum and maximum, and the open circle within the box marks the median. All the EC results

involved were measured by IMPROVE-A.

The discussions above raised a question that why the extraction significantly reduced EC_{max} for the HV samples. In principle, two factors could be responsible for the non-linear dependence of ATN on EC_s, including gradual saturation of ATN with increasing filter loading (the traditional explanation; Subramanian et al., 2006) and overestimation of EC mass. The EC_{max} of untreated samples corresponded to an ATN of 2.1, indicating that the saturation was presumably not a concern for the ATN results below this value. Regarding the extracted samples showing evidence for the loading effect (i.e., the targeted samples), ATN stayed below 2.1 for nearly all of them (28 out of 31), thus their non-linear ATN vs. EC_s dependences should be primarily attributed to the overestimation of EC mass rather than the saturation of ATN. Compared to the other extracted samples, the targeted ones were characterized by substantially higher sulfate loadings (Figure 3c). It was inferred that in addition to EC, the abundant sulfate was also a non-negligible contributor to ATN (e.g., through backward scattering; Petzold et al., 2005; Collaud Coen et al., 2010). Thus when ~~these~~ the targeted samples were heated in the carbon analyzer, volatilization of sulfate would lead to a decrease in ATN, i.e., an increase in filter transmittance signal. This was expected to result in a premature split of OC and EC, and eventually an overestimation of EC. Other scattering components such as nitrate and secondary organic aerosol (SOA) were not ~~considered~~ discussed here, since they were typically considered soluble in methanol and should be absent in the extracted filters.

Comparison of EC between the targeted samples and the corresponding untreated ones (i.e., the targeted group) showed an overall increasing trend after the extraction (Figure 3d). For these pairs of wintertime HV filters, the ratio of $EC_{extracted}$ (i.e., EC measured in the extracted samples) to $EC_{untreated}$ (i.e., EC measured in the untreated samples) averaged 1.16 $\pm$0.20. The extraction-induced

243 increase in EC coincided with the overestimation of elemental carbon mass by $EC_{extracted}$, which was
244 inferred to be associated with the presence of abundant sulfate in the extracted filters.

245 For the other pairs of wintertime HV samples (i.e., the reference group), the $EC_{extracted}$ to
246 $EC_{untreated}$ ratios averaged 0.80 ± 0.12, pointing to a decrease in EC after the extraction (Figure 3d).
247 This was also the case for all the LV samples collected during the winter campaign, with comparable
248 $EC_{extracted}$ to $EC_{untreated}$ ratios (averaging 0.78 ± 0.12). Here the LV samples were not divided into
249 subgroups because non-linear dependence of ATN on EC_s was identified neither before nor after the
250 extraction (Figure S2). Given that the loss of insoluble carbon (e.g., EC) was negligible for our
251 extraction procedures (Figure 2 and Cheng et al., 2024), the extraction-induced decrease of EC
252 likely pointed to the underestimation of elemental carbon mass by $EC_{extracted}$. A common feature for
253 the HV samples in the reference group and the entirety of the LV samples was the relatively low
254 sulfate loadings. Cheng et al. (2024) inferred that small amounts of sulfate likely favored the
255 transmission of light through the extracted filters (e.g., by forward scattering; Petzold et al., 2005;
256 Collaud Coen et al., 2010). In this case, when the extracted samples were heated during thermal-
257 optical analysis, volatilization of sulfate would induce a drop of filter transmittance signal, which
258 could not be distinguished from that caused by the formation of char-OC. This was expected to
259 result in an overcorrection for char-OC, i.e., an underestimation of EC.

260 The contrasting $EC_{extracted}$ to $EC_{untreated}$ ratios observed for the two groups of wintertime HV
261 samples suggested that the influence of sulfate on the transmittance signal of the extracted filter was
262 likely loading-dependent. ~~The influence was inferred to be dominated by forward scattering when~~
263 ~~sulfate was less abundant (e.g., for the reference group), whereas by backward scattering with~~
264 ~~relatively high sulfate loadings (e.g., for the targeted group).~~ The influence was inferred to be

dominated by backward scattering with relatively high sulfate loadings (e.g., for the targeted group), whereas by forward scattering when sulfate was less abundant (e.g., for the reference group). This inference was supported by the comparison of evolution patterns of filter transmittance signal under different sulfate loadings (Figure 4). For the extracted filter with abundant sulfate (i.e., Sample-A in Figure 4), the transmittance signal was largely unchanged during the He mode despite the sufficient organic carbon loading. Correspondingly, the operationally-defined char-OC only accounted for a relatively small fraction of the carbon evolving during the He/O_2 mode (i.e., He/O_2 carbon). A possible explanation was that as the sample was heated, the drop of *I* induced by char-OC was compensated by the increase of *I* due to the reduction in sulfate-driven backward scattering. For the extracted filter with relatively small amount of sulfate (i.e., Sample-B in Figure 4), however, the transmittance signal decreased significantly during the He mode, and the char-OC contribution to He/O_2 carbon became more considerable correspondingly. Given the much lower organic carbon loading for this sample (e.g., ~70% lower than Sample-A), the decrease of *I* was likely contributed by not only the formation of char-OC but also the reduction in sulfate-driven forward scattering. The $EC_{extracted}$ results appeared to be biased by different artifacts in ~~these two~~ the high- and low-sulfate cases, resulting in ~~underestimations or~~ overestimations or underestimations of elemental carbon mass, respectively. The sulfate-induced artifacts for $EC_{extracted}$ could be more directly reflected by the positive dependence of the $EC_{extracted}$ to $EC_{untreated}$ ratio on sulfate loading. As shown in Figure 5, the turning point for the artifact shifting from an underestimation to overestimation of elemental carbon mass by $EC_{extracted}$ occurred in the sulfate loading range of 10–15 μg/cm^2. Figure 5 also suggested that the artifacts for $EC_{extracted}$ were difficult to be accounted for, e.g., by a constant correction factor. This prohibited the use of $EC_{extracted}$ for further analysis of aerosol composition

and sources.

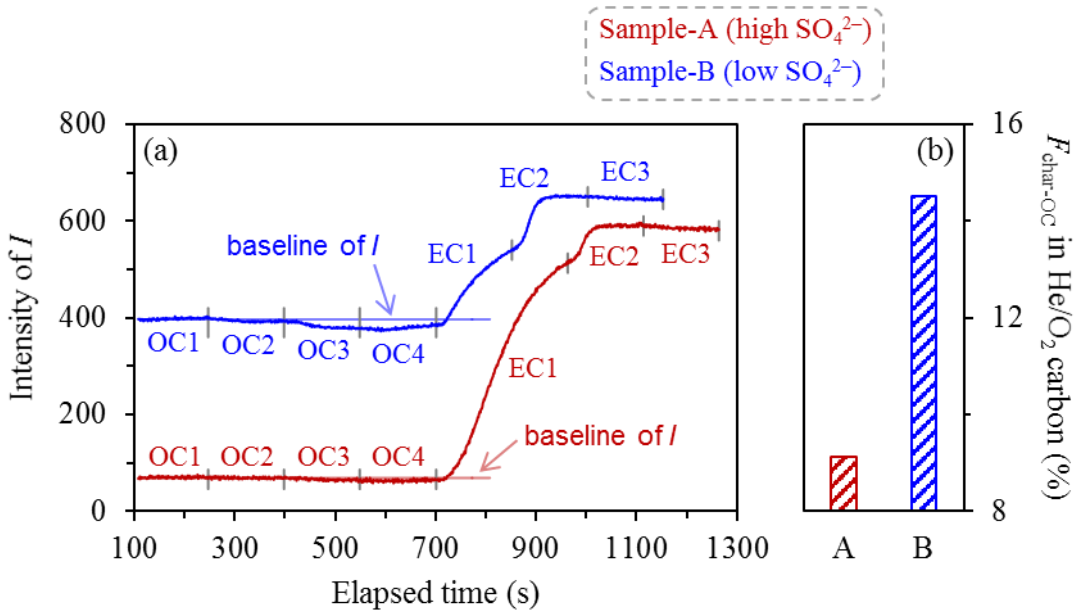

Figure 4. Comparisons of **(a)** the evolution patterns of filter transmittance signal (*I*) and **(b)** the fractions of char-OC (i.e., $F_{char\text{-}OC}$) in He/O_2 carbon for two extracted HV samples with relatively high and low sulfate loadings (namely Sample-A and Sample-B, respectively). The two samples were collected during the daytime of 25 January and the nighttime of 6 January, 2021, respectively. They had sulfate loadings of 13.21 and 3.29 μg/cm^2, and organic carbon loadings of 3.10 and 0.86 μgC/cm^2, respectively. The temperature protocol used was IMPROVE-A, in which the filter was first heated to 580 ℃ in a He atmosphere and then to 840 ℃ in a He/O_2 atmosphere. The two modes had 4 (i.e., OC1 to OC4) and 3 (i.e., EC1 to EC3) heating stages, respectively. He/O_2 carbon indicated the amount of carbon evolving during the oxidizing mode, and was typically comprised of char-OC and EC for IMPROVE-A.

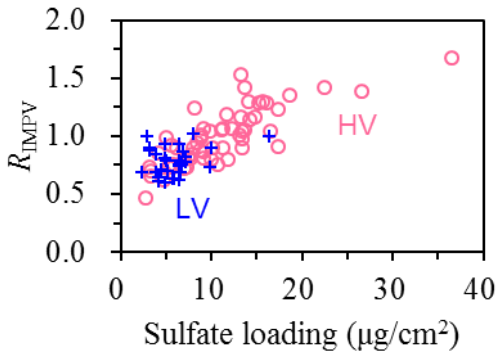

Figure 5. Dependence of R_{IMPV}, i.e., the $EC_{extracted}$ to $EC_{untreated}$ ratio determined by IMPROVE-A, on sulfate loading in winter. Consistent trends were observed by the HV and LV samples. The relatively wide range of R_{IMPV} (approximately 0.5–1.5) provided solid evidence for the invalidation of the $EC_{extracted}$ to $EC_{untreated}$ ratio as an indicator for the extraction-induced loss of EC.

For the untreated filters, ATN exhibited a strong linear correlation with EC_s for both HV and

LV, with three heavily-loaded HV samples as the only exception. Actually, for the three samples, their ATN vs. EC_s relationships did not deviate markedly from the regression line determined for the lower EC_s loadings. Therefore, we suggested that when applying IMPROVE-A to the winter samples, the measurement uncertainties should be less significant for $EC_{untreated}$ compared to $EC_{extracted}$.

The same conclusion could be reached by interpreting the OC to EC ratios (OC/EC). It has been widely accepted that OC/EC depended strongly on SOA formation, after excluding the ~~distinct~~ events impacted by irregular emissions such as fireworks and open burning. Such events were not evident throughout the winter campaign, and thus OC/EC was expected to increase with the enhancement of secondary aerosol production. Here we used the relative abundance of secondary inorganic ions (sulfate, nitrate and ammonium, i.e., SNA) compared to carbon monoxide (a typical primary species), i.e., the SNA/CO ratio, as an indicator for the significance of secondary aerosols. A benefit of using SNA/CO was that it was independent of EC measurement. The OC/EC ratio corresponding to $EC_{untreated}$ [i.e., $(OC/EC)^*$] was determined directly by the thermal-optical results from the untreated samples. For $EC_{extracted}$, the corresponding OC/EC [i.e., $(OC/EC)^\#$] was calculated as $(TC_{untreated} - EC_{extracted})/ EC_{extracted}$, where $TC_{untreated}$ indicates the total carbon concentration measured before the extraction. As shown in Figure 6 for the wintertime HV samples, $(OC/EC)^*$ exhibited reasonable accordance with SNA/CO (r = 0.72) but $(OC/EC)^\#$ did not (r = 0.02). The clear association between $(OC/EC)^*$ and SNA/CO, which was also supported by the results from LV (r = 0.66; Figure S3), provided additional evidence for the robustness of $EC_{untreated}$ determined by IMPROVE-A.

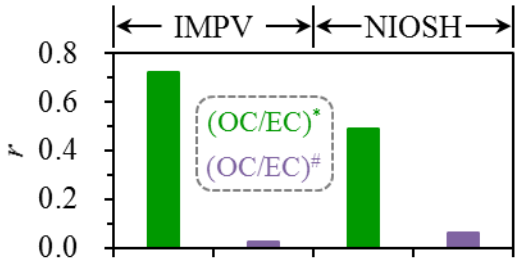

Figure 6. Comparison of *r* values derived from the linear regressions of various OC/EC estimations on SNA/CO, based on the wintertime HV samples. IMPV indicates the IMPROVE-A temperature protocol. A total of four sets of OC/EC ratios were determined using different protocols and pre-treatment approaches. The OC/EC ratio measured by the untreated samples using IMPROVE-A, i.e., the IMPV-based $(OC/EC)^{*}$, exhibited the strongest association with SNA/CO.

Compared to IMPROVE-A, NIOSH led to weaker correlations between $(OC/EC)^{*}$ and SNA/CO, as indicated by the smaller *r* values determined (0.49 vs. 0.72 for HV and 0.18 vs. 0.66 for LV; Figures 4 and S3). In addition, the NIOSH-based $(OC/EC)^{\#}$ did not exhibit apparent dependence on SNA/CO either (r = 0.06 and 0.34 for HV and LV, respectively). Thus Figures 6 and S3 clearly reflected the limitations of NIOSH-based OC/EC and thus NIOSH-based EC, further highlighting the benefit of using $EC_{untreated}$ determined by IMPROVE-A.

3.2 Evaluation of EC results from the spring campaign

In this section we evaluated the EC results from April, also starting with the HV samples analyzed by IMPROVE-A. To highlight the role of agricultural fires, we first separated the April samples into two groups (namely the fire-impacted and typical samples), which were characterized by considerable and insignificant impacts of open burning, respectively. As described in Supporting Information, the criteria for fire-impacted samples could be simplified as a levoglucosan to $TC_{untreated}$ ratio (f_{LG}; on a basis of carbon mass) of above 1.8%, based on a synthesis of f_{LG}, the levoglucosan to water-soluble potassium ratio (LG/K^{+}) and satellite-based fire hotspots (Figure S4). Before filter extraction, the dependence of ATN on EC_s could be approximated by a liner function (with a slope of 33.4 ± 1.5 m^2/gC and a close-to-zero intercept; r = 0.97) for all the typical samples

and the majority of the fire-impacted ones (Figure 7a), leading to an EC_{max} of 8 μgC/cm^2. For three of the fire-impacted samples, EC_s exceeded this threshold value and the ATN vs. EC_s relationships were found to deviate significantly from the regression line, especially for the two samples with EC_s above 10 μgC/cm^2 (as highlighted in Figure 7a).

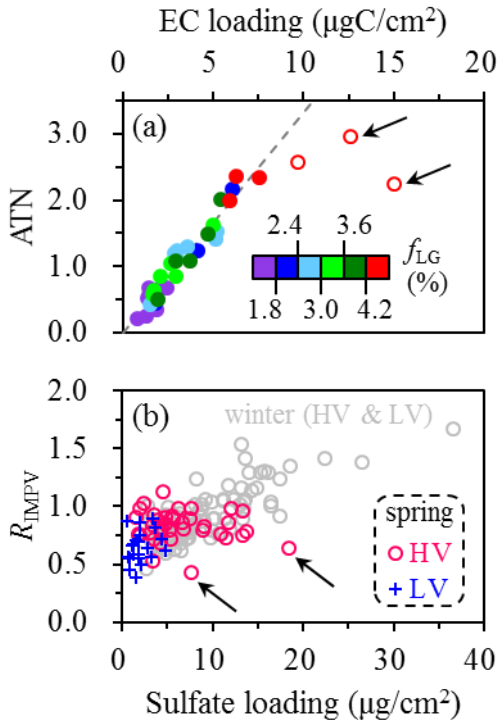

Figure 7. (a) Dependence of ATN on EC loading (EC_s) for the untreated HV samples collected in spring, color-coded by f_{LG} levels. Samples with linear and non-linear ATN vs. EC_s dependence are shown by the solid and open circles, respectively. f_{LG} values higher than 1.8% indicated significant impacts of agricultural fires. **(b)** Dependence of R_{IMPV}, i.e., the $EC_{extracted}$ to $EC_{untreated}$ ratio, on sulfate loading in spring. Results from winter were also shown for comparison. In general, a consistent relationship was observed between R_{IMPV} and sulfate loading for the samples, including both HV and LV, from different seasons. ~~The only exceptions were two~~ Two HV samples collected in spring were identified as outliers, as highlighted by the arrows. ~~The two distinct samples~~ The outlier samplers were also highlighted in (a), corresponding to the two points showing significant non-linear dependences of ATN on EC loading. All the EC results involved were measured by IMPROVE-A.

To elucidate factors responsible for the observed non-linear dependence of ATN on EC_s, we compared EC results from the untreated and extracted filters. Given the relatively low sulfate loadings observed throughout April (Figure 7b), it was with expectation that EC generally decreased

after the extraction. After excluding the results from two outliers (Figure 7b) ~~distinct samples~~, the $EC_{extracted}$ to $EC_{untreated}$ ratios averaged 0.84 ± 0.11, comparable to results from the reference group in winter. The two outlier ~~distinct~~ samples, which were collected on the nights of April 10 and 20, 2021, showed $EC_{extracted}$ to $EC_{untreated}$ ratios of as low as 0.64 and 0.43, respectively. Such significant extraction-induced decreases in EC could hardly be explained by the interference from sulfate in thermal-optical analysis of the extracted filters (Figure 7b). Instead, the two outlier ~~distinct~~ samples were found to show several noteworthy features: (i) they corresponded to the two samples showing significant non-linear ATN vs. EC_s dependences before the extraction (Figure 7a); (ii) their f_{LG} levels were at the higher end of the fire-impacted samples (with levoglucosan concentrations exceeding 7 μg/m^3), indicating extremely strong impacts of open burning (Figure 7a); (iii) their LG/K^+ ratios (> 1.7) were also at the higher end of the fire-impacted samples, which were characteristic of the emissions from smoldering combustion (Gao et al., 2003; Sullivan et al., 2019); (iv) their ATN decreased apparently after the extraction, by ~1.0 which were about one order of magnitude higher than results from the typical samples (~0.1). Thus it was inferred that $EC_{untreated}$ of the outlier ~~distinct~~ samples likely involved some light-absorbing organic compounds (i.e., BrC) emitted by agricultural fires with relatively low combustion efficiencies, and the absorption capacities of these organics were strong enough to make them a considerable contributor to ATN measured at 632 nm. Indeed, the BrC-related overestimation of elemental carbon mass was expected to be reduced considerably after the extraction. However, such overestimation seemed ~~apparent~~ significant only for the two outlier ~~distinct~~ samples (Figure 7a). In addition, recalling the lower-than-one $EC_{extracted}$ to $EC_{untreated}$ ratios observed for the other April samples (i.e., the sulfate-related artifact raised for the extracted filters), the methanol extraction actually brought little benefit for the determination of EC by

IMPROVE-A.

Unlike HV, all the LV samples showed a consistent relationship between ATN and EC_s before the extraction (Figure S5). It appeared that the strongly absorbing organics that could interfere EC measurement were mainly concentrated in some agriculture-fire smoke emitted at night (as indicated by the two outlier ~~distinct~~ HV samples), whereas their influence on EC determination was considerably weakened for the 24-h integrated LV samples. Thus the linear ATN vs. EC_s dependence, which was valid for all the untreated LV samples analyzed by IMPROVE-A, provided little evidence for the necessity of methanol extraction.

We also investigated the OC/EC vs. f_{LG} relationship for the HV samples collected in April. Open burning was considered to be favorable for the increase of ambient OC/EC, since the aerosols emitted were frequently found to be almost entirely organic (Liu et al., 2016; Garofalo et al., 2019; Gkatzelis et al., 2024). Then it was not surprising to observe a moderate correlation between $(OC/EC)^*$ and f_{LG} (r = 0.59; Figure 8), i.e., an increasing trend of $(OC/EC)^*$ with stronger impacts of agricultural fires. In addition, $(OC/EC)^*$ also depended moderately on SNA/CO (r = 0.49; Figure 8). This was with expectation as well, given the observational evidence on the concurrent enhancements of secondary inorganic and organic aerosols (e.g., Liu et al., 2020; Cheng et al., 2022). Replacing $(OC/EC)^*$ with $(OC/EC)^\#$ did not effectively strengthen the association of OC/EC with f_{LG} or SNA/CO (Figure 8). This conclusion also held for the LV samples (Figure 8). In summary, we did not observe additional evidence supporting the incorporation of methanol extraction with IMPROVE-A.

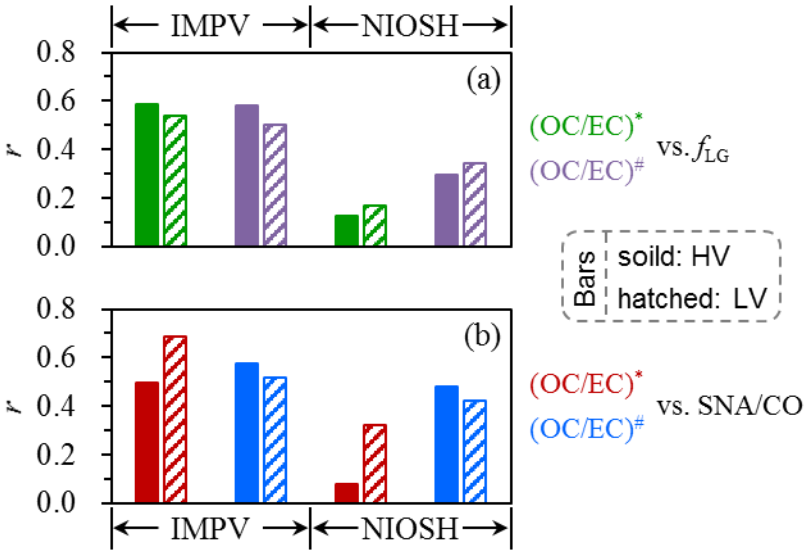

409

410 **Figure 8.** Comparisons of *r* values derived from the linear regressions of various OC/EC estimations
411 on **(a)** f_{LG} and **(b)** SNA/CO, based on the spring samples. IMPV indicates the IMPROVE-A
412 temperature protocol. Results from the HV and LV filters are shown by solid and hatched bars,
413 respectively. For both HV and LV, a total of four sets of OC/EC ratios were determined using
414 different protocols and pre-treatment approaches. In general, OC/EC ratios measured by the
415 untreated samples using IMPROVE-A, i.e., the IMPV-based $(OC/EC)^{*}$, exhibited reasonable
416 associations with aerosol sources. Using other OC/EC estimations failed to or did not effectively
417 enhance the associations.

418 Compared to $(OC/EC)^{*}$ determined by IMPROVE-A, the NIOSH-based $(OC/EC)^{*}$ and
419 $(OC/EC)^{\#}$ were less indicative of aerosol sources which could be reflected by f_{LG} and SNA/CO. This
420 was the case for both the HV and LV samples (Figure 8). Based on the discussions above, $EC_{untreated}$
421 determined by IMPROVE-A (EC^{*}) was also recommended for the conditions with prevalence of
422 agricultural fires (i.e., April), in line with the conclusion derived for winter. In addition, it should be
423 kept in mind that EC^{*} could overestimate elemental carbon mass due to the interference from
424 strongly absorbing BrC. However, such overestimation was generally uncommon, i.e., was
425 ~~considerable~~ significant only for some nighttime samples under extremely strong influences of low-
426 efficiency agricultural fires (as indicated by the two ~~distinct~~ HV samples identified as outliers;
427 Figure 7).

428 **3.3 Comparison of measurement results from the HV and LV samplers**

As mentioned in the Methods section, each LV sample corresponded to a pair of daytime and nighttime HV samples, indicating that measurement results from the HV samples could be averaged and then compared to those determined by LV. Here the inter-sampler comparison was performed for several components that are of broad interest in field observations, including elemental and organic carbon, secondary inorganic ions (sulfate, nitrate and ammonium), other water-soluble ions (potassium and chloride), organic tracer for biomass burning (levoglucosan), BrC mass concentration and light absorption coefficient. Based on the evaluation results in previous sections, EC^* and the corresponding OC, i.e., OC^* (measured before the extraction using IMPROVE-A), were selected for the comparison. In addition, following Cheng et al. (2024), BrC mass was calculated as the difference in TC between the untreated and extracted filters, while BrC absorption was investigated at a wavelength of 365 nm, i.e., $(b_{abs})_{365}$.

As shown in Figure 9, the two samplers generally led to comparable measurement results for all the species investigated. For example, the LV-to-HV ratios typically fell within the range of 0.8–1.2, i.e., results from the two samples generally agreed within ±20%. However, it was noticed that K^+ was the only component with the majority of the LV results lower than HV. In addition, the LV-to-HV ratio of K^+ was found to depend positively on the ratio of $PM_{2.5}$ to PM_{10} (Figure 10a). The $PM_{2.5}$ to PM_{10} ratio was strongly associated with the influence of dust, typically exhibiting a decreasing trend as the impact of dust became stronger (Putaud et al., 2010). Thus the events with decreased LV-to-HV ratios of K^+ (all of which occurred in spring) presumably coincided with dust episodes, when relatively large particles were expected to be a non-negligible contributor to K^+ (Wang et al., 2014a). Then a likely cause for the dependence shown in Figure 8a was that the impactor performances (e.g., the size-cut curves) were ~~different~~ not exactly the same for the two

samplers, such that some relatively large particles, if present, could be more effectively collected onto the HV filters ~~but would be removed by the impactor of~~ compared to LV.

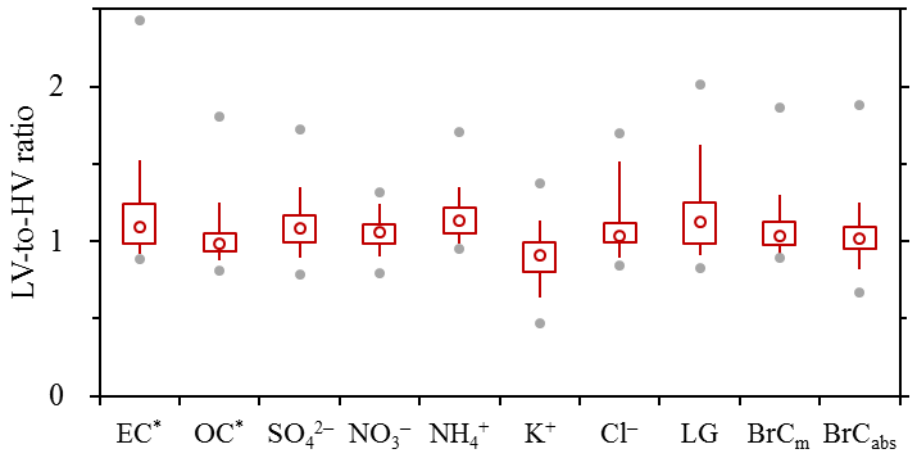

Figure 9. The LV-to-HV ratios determined for various species. BrC_m and BrC_{abs} indicate the mass concentration and $(b_{abs})_{365}$ of brown carbon, respectively.

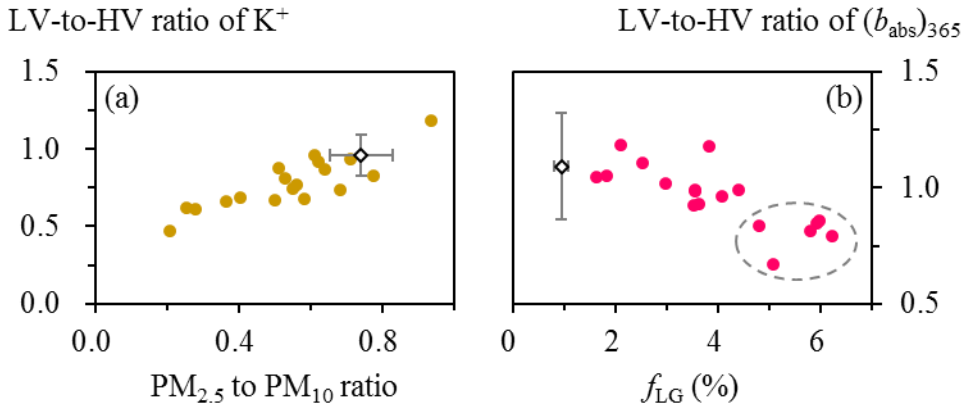

Figure 10. **(a)** Dependence of the LV-to-HV ratio of K^+ on the $PM_{2.5}$ to PM_{10} ratio. **(b)** Dependence of the LV-to-HV ratio of $(b_{abs})_{365}$ on f_{LG}. Results from spring are shown on a sample-by-sample basis, as indicated by the solid circles. For winter, only the average results are shown as indicated by the diamonds. In (b), the events with substantially lower LV-to-HV ratios of $(b_{abs})_{365}$ are highlighted by the dashed oval.

In addition, it was noticed that although the two samplers led to generally comparable $(b_{abs})_{365}$ results, the corresponding LV-to-HV ratios decreased substantially (e.g., down to 0.67) for the episodes with extremely strong impacts of agricultural fires (Figure 10b). A possible explanation was that some fire-emitted chromophores were ~~more or less distributed on~~ associated with relatively

large particles that would be more effectively collected onto the HV filters ~~removed by the inlet of LV but could pass through that of HV~~. Although these chromophores represented an important contributor to BrC absorption, their influence on BrC mass was likely insignificant, as indicated by the little influence of agricultural fires on the LV-to-HV ratio of BrC mass (Figure S6).

Finally, it should be noted that for the species except K^+ and $(b_{abs})_{365}$, their LV-to-HV ratios still showed different patterns of distribution (Figure 9). Analytical uncertainties should be partially responsible, e.g., as indicated by the more significant variations in the LV-to-HV ratios of EC^* compared to those of OC^*. Another likely cause was that the sampling duration of a given LV sample (24 hours) actually did not equal that of the corresponding HV (15 hours), which would result in different LV-to-HV ratios for the species with different diurnal cycles. In summary, many factors could be responsible for the inter-sampler discrepancies shown in Figure 9. Typically, the overall effects of these factors were higher LV-based concentrations than HV, with median LV-to-HV ratios concentrating in a relatively narrow range of 1–1.15. However, this comparability may not always hold. A possible explanation was that the impactor performances were more or less different between the two samplers, thus for specific components such as K^+ and some fire-emitted chromophores, this difference could exert a significant influence on their sampling.

4. Conclusions and implications

For the first time, EC results were compared among different sampling and analytical approaches based on field observations in Northeast China. Two samplers with flow rates of 1.13 m^3/min and 5 L/min were operated together during two distinct seasons, whereas thermal-optical analysis was performed by applying different protocols to both the untreated and extracted filters. Results from different seasons jointly suggested that $EC_{extracted}$ measured by IMPROVE-A (i.e.,

IMPV) was biased by complex artifacts associated with sulfate. The IMPV-based $EC_{extracted}$ tended to underestimate elemental carbon mass when sulfate was less abundant, whereas overestimations were evident at sufficiently high loadings of sulfate. The turning point for the artifact shifting from an underestimation to overestimation occurred in the sulfate loading range of 10–15 μg/cm^2. Such high sulfate loadings were rarely encountered by the LV samples and thus the corresponding IMPV-based EC typically decreased after the extraction (by ~20%). For the HV samples, their sulfate covered a wide range of ~2–35 μg/cm^2 during winter and in this case, the extraction-induced changes in EC usually varied between –50% and +50% for the IMPV-based results. ~~In addition to the complex sulfate-related artifacts, another problem identified for the IMPV-based $EC_{extracted}$ was that in winter, the corresponding OC/EC ratio exhibited relatively weak or even no association with the SNA/CO ratio, which was used as an indicator for the significance of secondary aerosol production. The NIOSH-based OC/EC occasionally showed acceptable correlation with SNA/CO, but it was never effectively enhanced by agricultural fire emissions.~~ In addition to the complex sulfate-related artifacts, another problem identified for the IMPV-based $EC_{extracted}$ was that the corresponding OC/EC ratio sometimes exhibited no association with the SNA/CO ratio, which was used as an indicator for the significance of secondary aerosol production. The NIOSH-based OC/EC ratios, determined by either $EC_{extracted}$ or $EC_{untreated}$, had the same problem. Then the IMPV-based $EC_{untreated}$ (EC^*) was recommended, as the corresponding OC/EC could always be reasonably linked to aerosol sources, e.g., secondary aerosol formation in winter and agricultural fire impacts (as reflected by f_{LG}) in spring.

Inter-sampler comparisons were performed for various species that are of broad interest in field observations, including EC^*. Although the flow rates differed by more than two orders of magnitude

between the two samplers, the LV and HV generally led to comparable measurement results for the majority of the species, with the median LV-to-HV ratios falling within a relatively narrow range of 1–1.15.

This study also raised two points that merit attentions. The first is that the IMPV-based $EC_{untreated}$, which was suggested for investigations on aerosol sources, might overestimate elemental carbon mass under extremely strong impacts of open burning. This problem was attributed to strongly absorbing BrC emitted by agricultural fires with relatively low combustion efficiencies. Although uncommon for the ambient samples in Harbin (a megacity located in a main agricultural region in China), this problem could introduce substantial uncertainties to the emission factors and thus inventories of biomass burning. We suggested that a key step to refine the EC measurement results was to concurrently minimize the inferences from strongly absorbing BrC and scattering components. Methanol extraction followed by water extraction of filter samples was expected to be a practical approach, which was worthy of further evaluations.

The second point was that some specific components should be interpreted with caution, even when comparing their measurement results from samplers with the same nominal cut-point. Our observational results indicated that some relatively large particles, if present, could be more effectively collected ~~onto the filters of~~ by the high-volume $PM_{2.5}$ sampler ~~but would be removed by the inlet of~~ compared to the low-volume one. This problem was attributed to the fact that the inlet performances (e.g., the size-cut curve) could not be exactly the same between the HV and LV $PM_{2.5}$ samplers. Among the various species involved in this study, this problem affected the measurements of K^+ as well as some fire-emitted chromophores in the fine mode. Thus we suggested that the K^+ results derived from different $PM_{2.5}$ samplers may not be directly comparable. In addition, although

we could not quantitatively determine the dust contribution to K^+ measured by the high-volume $PM_{2.5}$ sampler, K^+ should be used with caution as a biomass burning tracer for source apportionment studies relying on the HV-based observations.

By evaluating the observational results from different measurement approaches for species commonly used in source apportionment, this study contributed to the understanding of aerosol sources in Northeast China and thus the development of efficient haze pollution control strategies. Using the recommended OC and EC results together with levoglucosan (rather than K^+) as the biomass burning tracer, positive matrix factorization (PMF) analysis was performed for the 2020–2021 heating season based on a total of ~200 LV samples (including those involved in this study; Cheng et al., 2024). The concentrations of primary OC resolved were found to be in reasonable agreement with those predicted by an air quality model, when agricultural fires were absent. The consistency laid the foundation for the control policy focusing on primary aerosols. Cheng et al. (2024) also found that the model failed to reproduce the observed SOA levels, with large underestimations (by ~80%). Thus the observation-based source apportionment results were currently irreplaceable for evaluating the benefits of reducing SOA precursors. In summary, this study highlighted the importance of inter-method comparison for aerosol components (e.g., EC and K^+) that are of broad interest in field observations. Such efforts are expected to be more urgently needed for Northeast China, since this distinct region was recently targeted by the latest national-level pollution control policy in China (State Council, 2021) and thus is facing stronger demand for reducing $PM_{2.5}$.

Data availability. Data are available from the corresponding author upon request (jiumengliu@hit.edu.cn).

Author contributions. YC and JL designed the study and prepared the paper, with inputs from all the co-authors. YZ, ZZ and XC carried out the experiments.

Competing interests. The authors declare that they have no conflict of interest.

Disclaimer. Publisher's note: Copernicus Publications remains neutral with regard to jurisdictional claims made in the text, published maps, institutional affiliations, or any other geographical representation in this paper. While Copernicus Publications makes every effort to include appropriate place names, the final responsibility lies with the authors.

Acknowledgements. The authors thank Zhen-yu Du at the National Research Center for Environmental Analysis and Measurement and Lin-lin Liang at the Chinese Academy of Meteorological Sciences for their help in sample analysis.

Financial support. This research has been supported by the National Natural Science Foundation of China (42222706), the Natural Science Foundation of Heilongjiang Province (YQ2024D011), the State Key Laboratory of Urban Water Resource and Environment (2023DX10) and the Fundamental Research Funds for the Central Universities.

References

Aakko-Saksa, P., Koponen, P., Aurela, M., Vesala, H., Piimäkorpi, P., Murtonen, T., Sippula, O., Koponen, H., Karjalainen, P., Kuittinen, N., Panteliadis, P., Rönkkö, T., and Timonen, H.: Considerations in analysing elemental carbon from marine engine exhaust using residual, distillate and biofuels, ***J. Aerosol Sci.***, 126, 191–204, 2018.

Andela, N., Morton, D. C., Schroeder, W., Chen, Y., Brando, P. M., and Randerson, J. T.: Tracking and classifying Amazon fire events in near real time, ***Sci. Adv.***, 8, eabd2713, 2022.

Andreae, M. O., and Gelencsér, A.: Black carbon or brown carbon? The nature of light-absorbing carbonaceous aerosols, ***Atmos. Chem. Phys.***, 6, 3131–3148, 2006.

Buffaloe, G. M., Lack, D. A., Williams, E. J., Coffman, D., Hayden, K. L., Lerner, B. M., Li, S. M.,

578 Nuaaman, I., Massoli, P., Onasch, T. B., Quinn, P. K., and Cappa, C. D.: Black carbon
579 emissions from in-use ships: a California regional assessment, ***Atmos. Chem. Phys.***, 14, 1881–
580 1896, 2014.

581 Cavalli, F., Viana, M., Yttri, K. E., Genberg, J., and Putaud, J. P.: Toward a standardized thermal-
582 optical protocol for measuring atmospheric organic and elemental carbon: the EUSAAR
583 protocol, ***Atmos. Meas. Tech.***, 3, 79–89, 2010.

584 Chakrabarty, R. K., Shetty, N. J., Thind, A. S., Beeler, P., Sumlin, B. J., Zhang, C. C., Liu, P., Idrobo,
585 J. C., Adachi, K., Wagner, N. L., Schwarz, J. P., Ahern, A., Sedlacek, A. J., Lambe, A., Daube,
586 C., Lyu, M., Liu, C., Herndon, S., Onasch, T. B., and Mishra, R.: Shortwave absorption by
587 wildfire smoke dominated by dark brown carbon, ***Nat. Geosci.***, 16, 683–688, 2023.

588 Chang, X., Zhao, B., Zheng, H. T., Wang, S. X., Cai, S. Y., Guo, F. Q., Gui, P., Huang, G. H., Wu,
589 D., Han, L. C., Xing, J., Man, H. Y., Hu, R. L., Liang, C. R., Xu, Q. C., Qiu, X. H., Ding, D.,
590 Liu, K. Y., Han, R., Robinson, A. L., and Donahue, N. M.: Full-volatility emission framework
591 corrects missing and underestimated secondary organic aerosol sources, ***One Earth***, 5, 403–
592 412, 2022.

593 Chen, P. F., Kang, S. C., Tripathee, L., Ram, K., Rupakheti, M., Panday, A. K., Zhang, Q., Guo, J.
594 M., Wang, X. X., Pu, T., and Li, C. L.: Light absorption properties of elemental carbon (EC)
595 and water-soluble brown carbon (WS-BrC) in the Kathmandu Valley, Nepal: a 5-year study,
596 ***Environ. Pollut.***, 261, 114239, 2020.

597 Cheng, J., Tong, D., Zhang, Q., Liu, Y., Lei, Y., Yan, G., Yan, L., Yu, S., Cui, R. Y., Clarke, L., Geng,
598 G. N., Zheng, B., Zhang, X. Y., Davis, S. J., and He, K. B.: Pathways of China's $PM_{2.5}$ air
599 quality 2015-2060 in the context of carbon neutrality, ***Natl. Sci. Rev.***, 8, nwab078, 2021.

600 Cheng, Y., Cao, X. B., Yu, Q. Q., Liu, J. M., Ma, W. L., Qi, H., Zhang, Q., and He, K. B.: Synergy
601 of multiple drivers leading to severe winter haze pollution in a megacity in Northeast China,
602 ***Atmos. Res.***, 270, 106075, 2022.

603 Cheng, Y., Cao, X. B., Zhu, S. Q., Zhang, Z. Q., Liu, J. M., Zhang, H. L., Zhang, Q., and He, K. B.:
604 Exploring the sources of light-absorbing carbonaceous aerosols by integrating observational

and modeling results: insights from Northeast China, ***Atmos. Chem. Phys.***, 24, 9869–9883, 2024.

Chiappini, L., Verlhac, S., Aujay, R., Maenhaut, W., Putaud, J. P., Sciare, J., Jaffrezo, J. L., Liousse, C., Galy-Lacaux, C., Alleman, L. Y., Panteliadis, P., Leoz, E., and Favez, O.: Clues for a standardised thermal-optical protocol for the assessment of organic and elemental carbon within ambient air particulate matter, ***Atmos. Meas. Tech.***, 7, 1649–1661, 2014

Collaud Coen, M., Weingartner, E., Apituley, A., Ceburnis, D., Fierz-Schmidhauser, R., Flentje, H., Henzing, J. S., Jennings, S. G., Moerman, M., Petzold, A., Schmid, O., and Baltensperger, U.: Minimizing light absorption measurement artifacts of the Aethalometer: evaluation of five correction algorithms, ***Atmos. Meas. Tech.***, 3, 457–474, 2010.

Costa, V., Bacco, D., Castellazzi, S., Ricciardelli, I., Vecchietti, R., Zigola, C., and Pietrogrande, M. C.: Characteristics of carbonaceous aerosols in Emilia-Romagna (Northern Italy) based on two fall/winter field campaigns, ***Atmos. Res.***, 167, 100–107, 2016.

Dao, X., Lin, Y. C., Cao, F., Di, S. Y., Hong, Y. H., Xing, G. H., Li, J. J., Fu, P. Q., and Zhang, Y. L.: Introduction to the national aerosol chemical composition monitoring network of China: objectives, current status, and outlook, ***Bull. Am. Meteorol. Soc.***, 100, ES337–ES351, 2019.

Eckhardt, S., Pisso, I., Evangeliou, N., Zwaaftink, C. G., Plach, A., McConnell, J. R., Sigl, M., Ruppel, M., Zdanowicz, C., Lim, S., Chellman, N., Opel, T., Meyer, H., Steffensen, J. P., Schwikowski, M., and Stohl, A.: Revised historical Northern Hemisphere black carbon emissions based on inverse modeling of ice core records, ***Nat. Commun.***, 14, 271, 2023.

Fuzzi, S., Baltensperger, U., Carslaw, K., Decesari, S., van der Gon, H. D., Facchini, M. C., Fowler, D., Koren, I., Langford, B., Lohmann, U., Nemitz, E., Pandis, S., Riipinen, I., Rudich, Y., Schaap, M., Slowik, J. G., Spracklen, D. V., Vignati, E., Wild, M., Williams, M., and Gilardoni, S.: Particulate matter, air quality and climate: lessons learned and future needs, ***Atmos. Chem. Phys.***, 15, 8217–8299, 2015.

Garofalo, L. A., Pothier, M. A., Levin, E. J. T., Campos, T., Kreidenweis, S. M., and Farmer, D. K.: Emission and evolution of submicron organic aerosol in smoke from wildfires in the Western

United States, ***ACS Earth Space Chem.***, 3, 1237–1247, 2019.

Gao, C. Y., Heald, C. L., Katich, J. M., Luo, G., and Yu, F. Q.: Remote aerosol simulated during the Atmospheric Tomography (ATom) campaign and implications for aerosol lifetime, ***J. Geophys. Res. Atmos.***, 127, e2022JD036524, 2022.

Gao, S., Hegg, D. A., Hobbs, P. V., Kirchstetter, T. W., Magi, B. I., and Sadilek, M.: Water-soluble organic components in aerosols associated with savanna fires in southern Africa: identification, evolution, and distribution, ***J. Geophys. Res.***, 108, 8491, 2003.

Giannoni, M., Calzolai, G., Chiari,M., Cincinelli, A., Lucarelli, F., Martellini, T., and Nava, S.: A comparison between thermal-optical transmittance elemental carbon measured by different protocols in $PM_{2.5}$ samples, ***Sci. Total Environ.***, 571, 195–205, 2016.

Gkatzelis, G. I., Coggon, M. M., Stockwell, C. E., Hornbrook, R. S., Allen, H., Apel, E. C., Bela, M. M., Blake, D. R., Bourgeois, I., Brown, S. S., Campuzano-Jost, P., St. Clair, J. M., Crawford, J. H., Crounse, J. D., Day, D. A., DiGangi, J. P., Diskin, G. S., Fried, A., Gilman, J. B., Guo, H., Hair, J. W., Halliday, H. S., Hanisco, T. F., Hannun, R., Hills, A., Huey, L. G., Jimenez, J. L., Katich, J. M., Lamplugh, A., Lee, Y. R., Liao, J., Lindaas, J., McKeen, S. A., Mikoviny, T., Nault, B. A., Neuman, J. A., Nowak, J. B., Pagonis, D., Peischl, J., Perring, A. E., Piel, F., Rickly, P. S., Robinson, M. A., Rollins, A. W., Ryerson, T. B., Schueneman, M. K., Schwantes, R. H., Schwarz, J. P., Sekimoto, K., Selimovic, V., Shingler, T., Tanner, D. J., Tomsche, L., Vasquez, K. T., Veres, P. R., Washenfelder, R., Weibring, P., Wennberg, P. O., Wisthaler, A., Wolfe, G. M., Womack, C. C., Xu, L., Ball, K., Yokelson, R. J., and Warneke, C.: Parameterizations of US wildfire and prescribed fire emission ratios and emission factors based on FIREX-AQ aircraft measurements, ***Atmos. Chem. Phys.***, 24, 929–956, 2024.

Hand, J. L., Prenni, A. J., Raffuse, S. M., Hyslop, N. P., Malm, W. C., and Schichtel, B. A.: Spatial and seasonal variability of remote and urban speciated fine particulate matter in the United States, ***J. Geophys. Res. Atmos.***, 129, e2024JD042579, 2024

Hecobian, A., Zhang, X., Zheng, M., Frank, N., Edgerton, E. S., and Weber, R. J.: Water-soluble organic aerosol material and the light-absorption characteristics of aqueous extracts measured over the Southeastern United States, ***Atmos. Chem. Phys.***, 10, 5965–5977, 2010.

Hu, Z. F., Kang, S. C., Xu, J. Z., Zhang, C., Li, X. F., Yan, F. P., Zhang, Y. L., Chen, P. F., and Li, C. L.: Significant overestimation of black carbon concentration caused by high organic carbon in aerosols of the Tibetan Plateau, ***Atmos. Environ.***, 294, 119486, 2023.

Knox, A., Evans, G. J., Brook, J. R., Yao, X., Jeong, C. H., Godri, K. J., Sabaliauskas, K., and Slowik, J. G.: Mass absorption cross-section of ambient black carbon aerosol in relation to chemical age, ***Aerosol Sci. Technol.***, 43, 522–532, 2009.

Laborde, M., Schnaiter, M., Linke, C., Saathoff, H., Naumann, K. H., Möhler, O., Berlenz, S., Wagner, U., Taylor, J. W., Liu, D., Flynn, M., Allan, J. D., Coe, H., Heimerl, K., Dahlkötter, F., Weinzierl, B., Wollny, A. G., Zanatta, M., Cozic, J., Laj, P., Hitzenberger, R., Schwarz, J. P., and Gysel, M.: Single Particle Soot Photometer intercomparison at the AIDA chamber, ***Atmos. Meas. Tech.***, 5, 3077–3097, 2012.

Lack, D. A., Moosmüller, H., McMeeking, G. R., Chakrabarty, R. K., and Baumgardner, D.: Characterizing elemental, equivalent black, and refractory black carbon aerosol particles: a review of techniques, their limitations and uncertainties, ***Anal. Bioanal. Chem.***, 406, 99–122, 2014.

Lappi, M. K., and Ristimäki, J. M.: Evaluation of thermal optical analysis method of elemental carbon for marine fuel exhaust, ***J. Air Waste Manage. Assoc.***, 67, 1298–1318, 2017.

Li, H. Y., Lamb, K. D., Schwarz, J. P., Selimovic, V., Yokelson, R. J., McMeeking, G. R., and May, A. A.: Inter-comparison of black carbon measurement methods for simulated open biomass burning emissions, ***Atmos. Environ.***, 206, 156–169, 2019.

Li, J., Carlson, B. E., Yung, Y. L., Lv, D. R., Hansen, J., Penner, J. E., Liao, H., Ramaswamy, V., Kahn, R. A., Zhang, P., Dubovik, O., Ding, A. J., Lacis, A. A., Zhang, L., and Dong, Y. M.: Scattering and absorbing aerosols in the climate system, ***Nat. Rev. Earth Environ.***, 3, 363–379, 2022.

Liu J. M., Du Z. Y., Liang L. L., Yu Q. Q., Shen G. F., Ma Y. L., Zheng M., Cheng Y., and He K. B.: Uncertainties in thermal-optical measurements of black carbon: insights from source and ambient samples, ***Sci. Total Environ.***, 656, 239–249, 2019.

687 Liu, J. M., Wang, P. F., Zhang, H. L., Du, Z. Y., Zheng, B., Yu, Q. Q., Zheng, G. J., Ma, Y. L., Zheng,
688 M., Cheng, Y., Zhang, Q., and He, K. B.: Integration of field observation and air quality
689 modeling to characterize Beijing aerosol in different seasons, ***Chemosphere***, 242, 125195,
690 2020.

691 Liu, S. G., Geng, G. N., Xiao, Q. Y., Zheng, Y. X., Liu, X. D., Cheng, J., and Zhang, Q.: Tracking
692 daily concentrations of $PM_{2.5}$ chemical composition in China since 2000, ***Environ. Sci.***
693 ***Technol.***, 56, 16517–16527, 2022.

694 Liu, X. X., Zhang, Y., Huey, L. G., Yokelson, R. J., Wang, Y., Jimenez, J. L., Campuzano-Jost, P.,
695 Beyersdorf, A. J., Blake, D. R., Choi, Y., St Clair, J. M., Crounse, J. D., Day, D. A., Diskin, G.
696 S., Fried, A., Hall, S. R., Hanisco, T. F., King, L. E., Meinardi, S., Mikoviny, T., Palm, B. B.,
697 Peischl, J., Perring, A. E., Pollack, I. B., Ryerson, T. B., Sachse, G., Schwarz, J. P., Simpson, I.
698 J., Tanner, D. J., Thornhill, K. L., Ullmann, K., Weber, R. J., Wennberg, P. O., Wisthaler, A.,
699 Wolfe, G. M., and Ziemba, L. D.: Agricultural fires in the southeastern U.S. during SEAC^{4}RS:
700 Emissions of trace gases and particles and evolution of ozone, reactive nitrogen, and organic
701 aerosol, ***J. Geophys. Res. Atmos.***, 121, 7383–7414, 2016.

702 Petzold, A., Ogren, J. A., Fiebig, M., Laj, P., Li, S. M., Baltensperger, U., Holzer-Popp, T., Kinne,
703 S., Pappalardo, G., Sugimoto, N., Wehrli, C., Wiedensohler, A., and Zhang, X. Y.:
704 Recommendations for reporting “black carbon” measurements, ***Atmos. Chem. Phys.***, 13,
705 8365–8379, 2013.

706 Petzold, A., Schloesser, H., Sheridan, P. J., Arnott, W. P., Ogren, J. A., and Virkkula, A.: Evaluation
707 of multiangle absorption photometry for measuring aerosol light absorption, ***Aerosol Sci.***
708 ***Technol.***, 39, 40–51, 2005.

709 Philip, S., Martin, R., van Donkelaar, A., Lo, J. W. H., Wang, Y. X., Chen, D., Zhang, L., Kasibhatla,
710 P. S., Wang, S. W., Zhang, Q., Lu, Z., Streets, D. G., Bittman, S., and MacDonald, D. J.: Global
711 chemical composition of ambient fine particulate matter for exposure assessment, ***Environ.***
712 ***Sci. Technol.***, 48, 13060–13068, 2014.

713 Piazzalunga, A., Bernardoni, V., Fermo, P., Valli, G., and Vecchi, R.: Technical note: On the effect
714 of water-soluble compounds removal on EC quantification by TOT analysis in urban aerosol

715 samples, ***Atmos. Chem. Phys.***, 11, 10193–10203, 2011.

716 Pileci, R. E., Modini, R. L., Bertò, M., Yuan, J., Corbin, J. C., Marinoni, A., Henzing, B., Moerman,
717 M. M., Putaud, J. P., Spindler, G., Wehner, B., Müller, T., Tuch, T., Trentini, A., Zanatta, M.,
718 Baltensperger, U., and Gysel-Beer, M.: Comparison of co-located refractory black carbon (rBC)
719 and elemental carbon (EC) mass concentration measurements during field campaigns at several
720 European sites, ***Atmos. Meas. Tech.***, 14, 1379–1403, 2021.

721 Pöschl, U.: Atmospheric aerosols: composition, transformation, climate and health effects, ***Angew.***
722 ***Chem. Int. Ed.***, 44, 7520–7540, 2005.

723 Putaud, J. P., Van Dingenen, R., Alastuey, A., Bauer, H., Birmili, W., Cyrys, J., Flentje, H., Fuzzi,
724 S., Gehrig, R., Hansson, H. C., Harrison, R. M., Herrmann, H., Hitzenberger, R., Hüglin, C.,
725 Jones, A. M., Kasper-Giebl, A., Kiss, G., Kousa, A., Kuhlbusch, T. A. J., Löschau, G.,
726 Maenhaut, W., Molnar, A., Moreno, T., Pekkanen, J., Perrino, C., Pitz, M., Puxbaum, H.,
727 Querol, X., Rodriguez, S., Salma, I., Schwarz, J., Smolik, J., Schneider, J., Spindler, G., ten
728 Brink, H., Tursic, J., Viana, M., Wiedensohler, A., and Raes, F.: A European aerosol
729 phenomenology-3: Physical and chemical characteristics of particulate matter from 60 rural,
730 urban, and kerbside sites across Europe, ***Atmos. Environ.***, 44, 1308–1320, 2020.

731 Qin, Y. M., Tan, H. B., Li, Y. J., Li, Z. J., Schurman, M. I., Liu, L., Wu, C., and Chan, C. K.:
732 Chemical characteristics of brown carbon in atmospheric particles at a suburban site near
733 Guangzhou, China, ***Atmos. Chem. Phys.***, 18, 16409–16418, 2018.

734 Samset, B. H., Myhre, G., Herber, A., Kondo, Y., Li, S. M., Moteki, N., Koike, M., Oshima, N.,
735 Schwarz, J. P., Balkanski, Y., Bauer, S. E., Bellouin, N., Berntsen, T. K., Bian, H., Chin, M.,
736 Diehl, T., Easter, R. C., Ghan, S. J., Iversen, T., Kirkevåg, A., Lamarque, J. F., Lin, G., Liu, X.,
737 Penner, J. E., Schulz, M., Seland, Ø., Skeie, R. B., Stier, P., Takemura, T., Tsigaridis, K., and
738 Zhang, K.: Modelled black carbon radiative forcing and atmospheric lifetime in AeroCom
739 Phase II constrained by aircraft observations, ***Atmos. Chem. Phys.***, 14, 12465–12477, 2014.

740 Shen, G. F., Chen, Y. C., Wei, S. Y., Fu, X. F., Zhu, Y., and Tao, S.: Mass absorption efficiency of
741 elemental carbon for source samples from residential biomass and coal combustions, ***Atmos.***
742 ***Environ.***, 79, 79–84, 2013.

State Council: Circular on Further Promoting the Pollution Prevention and Control Battle, available at: https://www.gov.cn/zhengce/2021-11/07/content_5649656.htm, 2021.

Subramanian, R., Khlystov, A. Y., and Robinson, A. L.: Effect of peak inert-mode temperature on elemental carbon measured using thermal-optical analysis, ***Aerosol Sci. Technol.***, 40, 763–780, 2006.

Sullivan, A. P., Guo, H., Schroder, J. C., Campuzano-Jost, P., Jimenez, J. L., Campos, T., Shah, V., Jaeglé, L., Lee, B. H., Lopez-Hilfiker, F. D., Thornton, J. A., Brown, S. S., and Weber, R. J.: Biomass burning markers and residential burning in the WINTER aircraft campaign, ***J. Geophys. Res. Atmos.***, 124, 1846–1861, 2019.

Tinorua, S., Denjean, C., Nabat, P., Pont, V., Arnaud, M., Bourrianne, T., Dias Alves, M., and Gardrat, E.: A 2-year intercomparison of three methods for measuring black carbon concentration at a high-altitude research station in Europe, ***Atmos. Meas. Tech.***, 17, 3897–3915, 2024.

von Schneidemesser, E., Monks, P. S., Allan, J. D., Bruhwiler, L., Forster, P., Fowler, D., Lauer, A., Morgan, W. T., Paasonen, P., Righi, M., Sindelarova, K., and Sutton, M. A.: Chemistry and the linkages between air quality and climate change, ***Chem. Rev.***, 115, 3856–3897, 2015.

Wang, G. H., Cheng, C. L., Huang, Y., Tao, J., Ren, Y. Q., Wu, F., Meng, J. J., Li, J. J., Cheng, Y. T., Cao, J. J., Liu, S. X., Zhang, T., Zhang, R., and Chen, Y. B.: Evolution of aerosol chemistry in Xi'an, inland China, during the dust storm period of 2013 – Part 1: Sources, chemical forms and formation mechanisms of nitrate and sulfate, ***Atmos. Chem. Phys.***, 14, 11571–11585, 2014a.

Wang, R., Tao, S., Balkanski, Y., Ciais, P., Boucher, O., Liu, J. F., Piao, S. L., Shen, H. Z., Vuolo, M. R., Valari, M., Chen, H., Chen, Y. C., Cozic, A., Huang, Y., Li, B. G., Li, W., Shen, G. F., Wang, B., and Zhang, Y. Y.: Exposure to ambient black carbon derived from a unique inventory and high-resolution model, ***Proc. Natl. Acad. Sci. U. S. A.***, 111, 2459–2463, 2014b.

Wang, X., Heald, C. L., Liu, J. M., Weber, R. J., Campuzano-Jost, P., Jimenez, J. L., Schwarz, J. P., and Perring, A. E.: Exploring the observational constraints on the simulation of brown carbon,

770 ***Atmos. Chem. Phys.***, 18, 635–653, 2018.

771 Wei, J., Li, Z. Q., Lyapustin, A., Wang, J., Dubovik, O., Schwartz, J., Sun, L., Li, C., Liu, S., and
772 Zhu, T.: First close insight into global daily gapless 1 km $PM_{2.5}$ pollution, variability, and health
773 impact, ***Nat. Commun.***, 14, 8349, 2023.

774 Xiao, Q. Y., Geng, G. N., Xue, T., Liu, S. G., Cai, C. L., He, K. B., and Zhang, Q.: Tracking $PM_{2.5}$
775 and O_3 Pollution and the related health burden in China 2013-2020, ***Environ. Sci. Technol.***,
776 56, 6922–6932, 2022.

777 Yang, H., and Yu, J. Z.: Uncertainties in charring correction in the analysis of elemental and organic
778 carbon in atmospheric particles by thermal/optical methods, ***Environ. Sci. Technol.***, 36, 5199–
779 5204, 2002.

780 Yu, J. Z., Xu, J. H., and Yang, H.: Charring characteristics of atmospheric organic particulate matter
781 in thermal analysis, ***Environ. Sci. Technol.***, 36, 754–761, 2002.

782 Zheng, G. J., Duan, F. K., Su, H., Ma, Y. L., Cheng, Y., Zheng, B., Zhang, Q., Huang, T., Kimoto,
783 T., Chang, D., Pöschl, U., Cheng, Y. F., and He, K. B.: Exploring the severe winter haze in
784 Beijing: the impact of synoptic weather, regional transport and heterogeneous reactions, ***Atmos.***
785 ***Chem. Phys.***, 15, 2969–2983, 2015.

786 Zhong, Q. R., Schutgens, N., van der Werf, G. R., Takemura, T., van Noije, T., Mielonen, T., Checa-
787 Garcia, R., Lohmann, U., Kirkevåg, A., Oliviéé, D. J. L., Kokkola, H., Matsui, H., Kipling, Z.,
788 Ginoux, P., Le Sager, P., Rémy, S., Bian, H. S., Chin, M., Zhang, K., Bauer, S. E., and Tsigaridis,
789 K.: Threefold reduction of modeled uncertainty in direct radiative effects over biomass burning
790 regions by constraining absorbing aerosols, ***Sci. Adv.***, 9, eadi3568, 2023.